Electronic Supplementary Information (ESI) for Journal of Materials Chemistry C

Supporting Information

Achieving Highly Efficient Narrowband Sky-Blue Electroluminescence with Alleviated Efficiency Roll-off by Molecular-Structure Regulation and Device-Configuration Optimization

Xianju Yan,[a] Zhiqiang Li,[b] Qingyang Wang,[a] Yupei Qu,[a] Yincai Xu,*[,a] and Yue Wang[a,b]

[a] State Key Laboratory of Supramolecular Structure and Materials, College of Chemistry, Jilin University, Changchun 130012, P. R. China.

[b] Jihua Hengye Electronic Materials Co., Ltd. Foshan 528200, Guangdong Province, P. R. China.

General Information: Thermo Fisher ITQ1100 GC/MS mass spectrometer was employed to measure the mass spectra. Flash EA 1112 spectrometer was used to perform the elemental analysis. Bruker AVANCE III 500 and 600 MHz spectrometers were selected to measure the ^{1}H and $^{13}C\{^{1}H\}$ NMR spectra, respectively, with tetramethylsilane (TMS) as internal standard. Shimadzu RF-5301 PC spectrometer and Shimadzu UV-2550 spectrophotometers were adopted to record the PL emission spectra and UV–vis absorption, respectively. The fluorescence and phosphorescence spectra taken at liquid nitrogen temperature (77 K) were recorded by Ocean Optics QE Pro with 365 nm Ocean Optics LLS excitation source. Edinburgh FLS920 steady state fluorimeter equipping with an integrating sphere was employed to measure the absolute photoluminescence quantum yields of solution and film. FLS980 fluorescence lifetime measurement system with 365 nm LED excitation source was selected to investigate the transient PL decay. In the range of 25 to 800 °C, TA Q500 thermogravimeter was selected to perform the thermogravimetric analysis of target molecules under nitrogen at a heating rate of 10 K min^{-1}. BAS 100W Bioanalytical electrochemical work station was used to measure the electrochemical property with platinum disk as working electrode, platinum wire as auxiliary electrode, porous glass wick Ag/Ag^{+} as pseudo reference electrode and ferrocene/ferrocenium as internal standard. The oxidation (in anhydrous dichloromethane) and reduction (in anhydrous tetrahydrofuran) potential were measured at a scan rate of 100 mV s^{-1} using 0.1 M solution of n-Bu_4NPF_6 as supporting electrolyte.

Theoretical Calculations Method: The ground state geometries of gas state were fully optimized by B3LYP method including Grimme's dispersion correction with 6-31G(d,p) basis set using Gaussian 09 software package.[1-5] HOMO and LUMO were visualized with Gaussview 5.0. The excited state properties were calculated by TDDFT with the same theory level as DFT.

Calculation Equations of External Quantum Efficiency: When assuming the external emission profile is Lambertian distribution, the EQE can be determined by the following equations:

$$EQE = \frac{N_p}{N_e} \quad (1)$$

$$N_p = \frac{\int L_e(\lambda) \cdot W(\lambda) \cdot d\lambda}{h \times c} \times \pi \times D \quad (2)$$

$$N_e = \frac{I}{e} \tag{3}$$

Where N_p is the photons number, N_e is the electrons number, L_e (λ) is the spectral radiance (W sr^{-1} m^{-2} nm^{-1}), W (λ) is the wavelength, $d\lambda$ = 1, D is the emitting area, h is the Planck's constant, c is the speed of light in vacuum, e is the elementary charge of electron and I is the injected current.

Synthesis of Materials: All reagents were purchased from *Energy Chemical Co.* and immediately used without further purification. Schlenk technology was strictly performed under nitrogen conditions in all reactions. Synthesis Procedure was showed below in detail. The final product was first purified by column chromatography, then temperature-gradient vacuum sublimation was utilized to further purify the target compound.

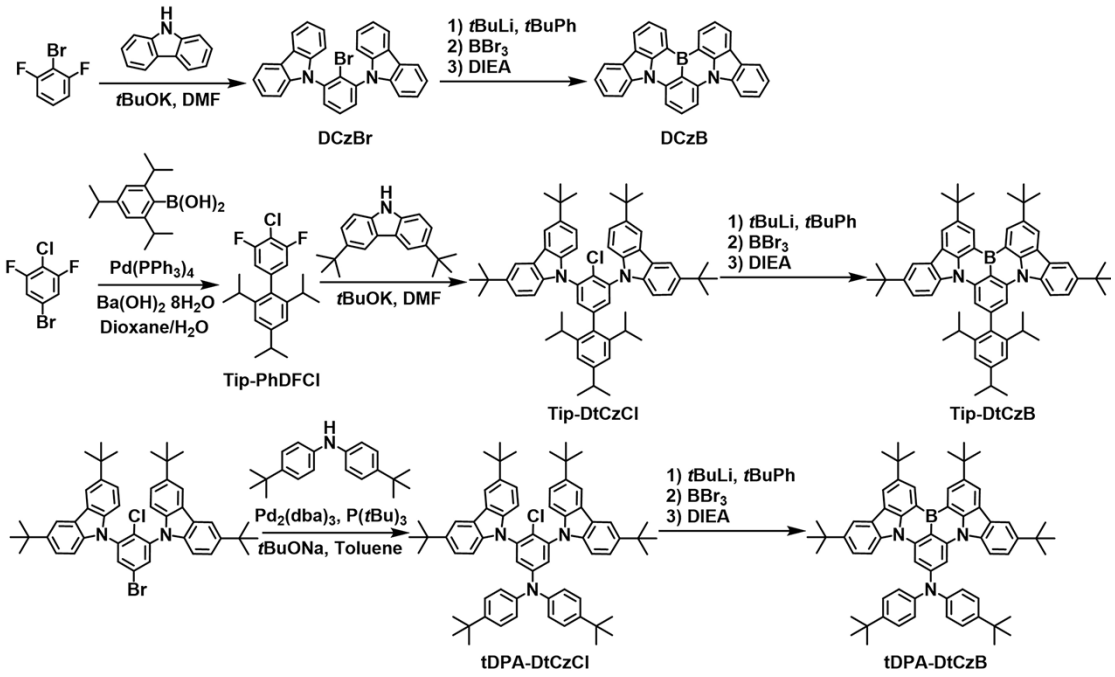

Scheme S1. Synthetic procedures of the investigated compounds.

Synthesis of 9,9'-(2-bromo-1,3-phenylene)bis(9*H*-carbazole) (DCzBr): 120 ml solution of anhydrous *N*,*N*-dimethylformamide (DMF) which contains 9*H*-carbazole (5.9 g, 35.2 mmol) was slowly added dropwise into a mixture of potassium *t*-butoxide (*t*BuOK) (5.4 g, 48.0 mmol) and 50 ml anhydrous DMF in a period of 15 min. After the system was stirring for 2 h at room temperature, 20 ml anhydrous DMF solution containing 2-bromo-

1,3-difluorobenzene (3.1 g, 16.0 mmol) was injected dropwise into it within 15 min. The solution was stirred at 140 °C for 24 h and then cooled down. The resulted solution was poured into ice water (500 g). The white powder solid was filtered out and dried in vacuum first, then it was further purified by column chromatography with using a mixture eluent of dichloromethane/petroleum ether (1:3), resulting in a white solid (6.2 g). Yield: 80 %. ^{1}H NMR (500 MHz, Chloroform-*d*) δ 8.21 – 8.13 (m, 4H), 7.76 (dd, *J* = 8.9, 6.6 Hz, 1H), 7.73 – 7.68 (m, 2H), 7.47 (ddd, *J* = 8.2, 7.2, 1.2 Hz, 4H), 7.35 – 7.31 (m, 4H), 7.20 (d, *J* = 8.1 Hz, 4H). ESI-MS (M): m/z: 486.83 $[M]^+$ (calcd: 487.40).

Synthesis of 2,6-bis(9*H*-carbazol-9-yl) boron (DCzB): A solution of *tert*-butyllithium (*t*BuLi) in n-pentane (19.4 mL, 1.3 M, 25.2 mmol) was added slowly to a solution of DCzBr (6.1 g, 12.6 mmol) in *tert*-butylbenzene (*t*BuPh) (100 mL) at 0 ºC under a nitrogen atmosphere. After stirring at 60 ºC for 2 h, n-pentane was removed in vacuum. After addition of boron tribromide (BBr_3) (2.4 mL, 25.2 mmol) at –30 ºC, the reaction mixture was stirred at room temperature for 1 h. *N*,*N*-Diisopropylethylamine (DIEA) (3.5 mL, 25.2 mmol) was added at 0 ºC and then the reaction mixture was allowed to room temperature. After stirring at 130 ºC for 6 h, the reaction mixture was cooled to room temperature. 10 ml methanol was added to the reaction mixture to quench residual BBr_3. The mixture was separated and extracted with dichloromethane and water. The combined organic layer was condensed in vacuum and purified by column chromatography with a mixture eluent of dichloromethane/petroleum ether (1:10), resulting in a yellow solid (1.0 g). Yield: 20 %. ^{1}H NMR (500 MHz, Chloroform-*d*) δ 8.98 (d, *J* = 7.5 Hz, 2H), 8.49 (d, *J* = 8.4 Hz, 2H), 8.37 (dd, *J* = 8.0, 4.2 Hz, 4H), 8.25 (d, *J* = 7.5 Hz, 2H), 8.02 (t, *J* = 8.3 Hz, 1H), 7.69 (t, *J* = 7.5 Hz, 2H), 7.62 (t, *J* = 8.1 Hz, 2H), 7.46 (t, *J* = 7.4 Hz, 2H). ^{13}C{^{1}H} NMR (151 MHz, Chloroform-*d*) δ 133.37, 126.92, 123.57, 122.42, 122.13, 121.03, 114.55, 108.72, 29.71. ESI-MS (M): m/z: $[M]^+$ 416.00 (calcd: 416.29). Anal. Calcd for $C_{30}H_{17}BN_2$: C, 86.56; H, 4.12; N, 6.73. Found: C, 86.76; H, 4.44; N, 6.64.

Synthesis of DtCzB: The synthetic process was referred to the reported literature.[6]

Synthesis of 4'-chloro-3',5'-difluoro-2,4,6-triisopropyl-1,1'-biphenyl (Tip-PhDFCl): 5-bromo-2-chloro-1,3-difluorobenzene (4.1 g, 18 mmol), (2,4,6-triisopropylphenyl)boronic acid (5.0 g, 20.0 mmol) and barium

hydroxide octahydrate ($Ba(OH)_2 \bullet 8H_2O$) (11.4 g, 36 mmol) were added to water (45 mL) and dioxane (135 mL). The mixture was bubbled with N_2 for further 10 minutes, and tetrakis(triphenylphosphine)palladium(0) ($Pd(PPh_3)_4$) (1.0 g, 0.9 mmol) was added under a high flow of N_2. Then the mixture was heated to reflux and stirred for 12 hours. After cooling to room temperature, the reaction mixture was extracted with dichloromethane and water, and the combined organic layer was condensed in vacuum, and then the crude product was further purified by column chromatography with using a mixture eluent of dichloromethane/petroleum ether (1:5) to afford a white solid (5.7 g). Yield: 91%. ^{1}H NMR (500 MHz, Chloroform-*d*), δ 7.05 (s, 2H), 6.86 – 6.79 (m, 2H), 2.93 (hept, *J* = 7.0 Hz, 1H), 2.53 (p, *J* = 6.9 Hz, 2H), 1.29 (d, *J* = 6.9 Hz, 6H), 1.10 (d, *J* = 6.9 Hz, 12H). ESI-MS (M): m/z: 350.01 [M]+ (calcd: 350.88).

Synthesis of 9,9'-(4-chloro-2',4',6'-triisopropyl-[1,1'-biphenyl]-3,5-diyl)bis(3,6-di-*tert*-butyl-9*H*-carbazole) (Tip-DtCzCl): 100 ml solution of anhydrous DMF which contains 3,6-di-*tert*-butyl-9*H*-carbazole (9.8 g, 35.2 mmol) was slowly added dropwise into a mixture of *t*BuOK (5.4 g, 48.0 mmol) and 50 ml anhydrous DMF in a period of 15 min. After the system was stirring for 2 h at room temperature, 20 ml anhydrous DMF solution containing Tip-PhDFCl (5.6 g, 16.0 mmol) was injected dropwise into it within 15 min. The solution was stirred at 140 °C for 24 h and then cooled down. The resulted solution was poured into ice water (500 g). The white powder solid was filtered out and dried in vacuum first, then it was further purified by column chromatography with using a mixture eluent of dichloromethane/petroleum ether (1:3), resulting in a white solid (11.3 g). Yield: 81 %. ^{1}H NMR (500 MHz, Chloroform-*d*) δ 8.15 (d, *J* = 1.9 Hz, 4H), 7.52 (d, *J* = 7.0 Hz, 6H), 7.23 (d, *J* = 8.6 Hz, 4H), 7.05 (s, 2H), 2.87 (dq, *J* = 13.8, 7.0 Hz, 3H), 1.47 (s, 36H), 1.26 (d, *J* = 6.9 Hz, 6H), 1.21 (d, *J* = 6.8 Hz, 12H). ESI-MS (M): m/z: 869.01 $[M]^+$ (calcd: 869.72).

Synthesis of 4-(2',4',6'-triisopropylbenzene)-2,6-bis(9*H*-carbazol-9-yl) boron (Tip-DtCzB): A similar procedure like synthesizing DCzB was carried out except replacing DCzBr with equivalent stoichiometric Tip-DtCzCl (11.0 g, 12.6 mmol), resulting in a yellowish green solid (4.0 g). Yield: 38 %. ^{1}H NMR (500 MHz, Chloroform-*d*) δ 9.16 (d, *J* = 5.5 Hz, 2H), 8.48 (d, *J* = 5.0 Hz, 2H), 8.25 (d, *J* = 6.4 Hz, 4H), 8.14 (d, *J* = 4.3 Hz, 2H), 7.57 (d, *J* = 8.0 Hz, 2H), 7.21 (s, 2H), 3.06 (p, *J* = 6.9 Hz, 1H), 2.90 (q, *J* = 6.7 Hz, 2H), 1.69 (s, 18H), 1.50 (s, 18H),

1.41 (d, *J* = 6.6 Hz, 6H), 1.19 (d, *J* = 6.5 Hz, 12H). $^{13}C\{^{1}H\}$ NMR (151 MHz, Chloroform-*d*) δ 148.42, 146.62, 145.34, 144.75, 144.03, 141.75, 138.31, 137.37, 129.87, 127.09, 124.45, 123.67, 120.88, 120.67, 117.25, 114.10, 109.85, 35.23, 34.80, 32.25, 31.83, 30.59, 24.69, 24.20. ESI-MS (M): m/z: 842.65 $[M]^+$ (calcd: 843.06). Anal. Calcd for $C_{61}H_{71}BN_2$: C, 86.91; H, 8.49; N, 3.32. Found: C, 86.95; H, 8.57; N, 3.21.

Synthesis of 9,9'-(5-bromo-2-chloro-1,3-phenylene)bis(3,6-di-*tert*-butyl-9*H*-carbazole): The synthesis process was referred to the reported literature.[7]

Synthesis of *N*,*N*-bis(4-(*tert*-butyl)phenyl)-4-chloro-3,5-bis(3,6-di-*tert*-butyl-9*H*-carbazol-9-yl)anilinet (DPA-DtCzCl): 9,9'-(5-bromo-2-chloro-1,3-phenylene)bis(3,6-di-*tert*-butyl-9*H*-carbazole) (10.8 g, 14.5 mmol), 4,4-di-*tert*-butyldiphenylamine (4.5 g, 16.0 mmol) and sodium *t*-butoxide (*t*BuONa) (3.5 g, 36.3 mmol) were added to toluene (120 mL). The mixture was bubbled with N_2 for further 10 minutes, tris(dibenzylideneacetone)dipalladium ($Pd_2(dba)_3$) (265.6 mg, 0.29 mmol) and tri-*tert*-butylphosphine($P(tBu)_3$) (146.7 mg, 0.73 mmol) were added under a high flow of N_2. Then the mixture was heated to reflux and stirred for 12 hours. After cooling to room temperature, the reaction mixture was extracted with dichloromethane and water, and the combined organic layer was condensed in vacuum, and then the crude product was further purified by column chromatography with using a mixture eluent of dichloromethane/petroleum ether (2:5) to afford a white solid (12.1 g). Yield: 88%. ^{1}H NMR (500 MHz, Chloroform-d), δ 8.10 (d, *J* = 2.0 Hz, 4H), 7.51 (dd, *J* = 8.7, 2.0 Hz, 4H), 7.29 – 7.25 (m, 4H), 7.24 – 7.20 (m, 6H), 7.14 – 7.09 (m, 4H), 1.46 (d, *J* = 0.8 Hz, 36H), 1.25 (d, *J* = 1.5 Hz, 18H). ESI-MS (M): m/z: 946.10 [M]+ (calcd: 946.81).

Synthesis of 4-(4',4'-di-*tert*-butyldiphenylamine)-2,6-bis(9*H*-carbazol-9-yl) boron (tDPA-DtCzB): A similar procedure like synthesizing DCzB was carried out except replacing DCzBr with equivalent stoichiometric tDPA-DtCzCl (11.9 g, 12.6 mmol), resulting in a yellowish green solid (2.9 g). Yield: 25 %. ^{1}H NMR (500 MHz, Chloroform-*d*) δ 9.05 (s, 2H), 8.37 (s, 2H), 8.18 (s, 2H), 7.73 (s, 2H), 7.62 (d, *J* = 9.1 Hz, 2H), 7.59 – 7.53 (m, 4H), 7.48 (d, *J* = 9.0 Hz, 4H), 7.30 (d, *J* = 8.8 Hz, 2H), 1.65 (s, 18H), 1.46 (dd, *J* = 7.8, 2.1 Hz, 36H). $^{13}C\{^{1}H\}$ NMR (151 MHz, Chloroform-*d*) δ 153.53, 148.41, 144.83, 144.30, 143.86, 141.76, 138.06, 129.64, 127.04, 126.71, 123.74, 123.26, 121.99, 119.86, 117.06, 113.64, 98.51, 35.12, 34.67, 32.22, 31.76, 31.53. ESI-MS (M): m/z: 919.80 $[M]^+$

(calcd: 920.15). Anal. Calcd for $C_{66}H_{74}BN_3$: C, 86.15; H, 8.11; N, 4.57. Found: C, 86.25; H, 8.24; N, 4.41.

Device Fabrication and Measurements: The indium tin oxide (ITO) glass substrates with a sheet resistance of 15 Ω per square were cleaned with optical detergent, deionized water, acetone and isopropanol successively, and then treated with plasma for 5 minutes. Subsequently, they were transferred to a vacuum chamber. Under high vacuum (< 9×10^{-5} Pa), the organic materials were deposited onto the ITO glass substrates at a rate of 0.5 Å s^{-1}. After finishing the deposition of organic layers, ITO glass substrates were patterned by a shadow mask with an array of 2.0 mm × 2.5 mm openings. Then LiF and Al were successively deposited at a rate of 0.1 Å s^{-1} and 5 Å s^{-1}, respectively. The EL spectrum, CIE coordinates and luminance intensity of OLEDs were recorded by Photo Research PR655, meanwhile, the current density (*J*) and driving voltage (*V*) were recorded by Keithley 2400. By assuming Lambertian distribution, EQE was estimated according to brightness, electroluminescence spectrum and current density. The materials of device fabrication are provided by Xi'an Polymer Light Technology Corp.

Calculation Formulas for the Photophysical Parameters: The calculation formulas for the rate constant of fluorescence (k_F), internal conversion (k_{IC}), intersystem crossing (k_{ISC}), TADF (k_{TADF}) and reverse intersystem crossing (k_{RISC}) are expressed as following list:[8–11]

$$k_F = \Phi_F/\tau_F \quad \text{(S1)}$$
$$\Phi_{PL} = k_F/(k_F + k_{IC}) \quad \text{(S2)}$$
$$\Phi_F = k_F/(k_F + k_{IC} + k_{ISC}) \quad \text{(S3)}$$
$$\Phi_{ISC} = k_{ISC}/(k_F + k_{IC} + k_{ISC}) \quad \text{(S4)}$$
$$k_{TADF} = \Phi_{TADF}/(\Phi_{ISC}\,\tau_{TADF}) \quad \text{(S5)}$$
$$k_{RISC} = k_F\,k_{TADF}\,\Phi_{TADF}/(k_{ISC}\,\Phi_F) \quad \text{(S6)}$$
$$\Phi_{TADF}/\Phi_F = (\Phi_{ISC}\,\Phi_{RISC})/(1-\Phi_{ISC}\,\Phi_{RISC}) \quad \text{(S7)}$$

Where Φ_{PL} is the total fluorescence quantum yield, Φ_F is the prompt fluorescent component of Φ_{PL}, Φ_{TADF} is the delayed fluorescent component of Φ_{PL}. τ_F is the lifetime of prompt fluorescence, τ_{TADF} is the lifetime of TADF. k_F is the rate constant of fluorescence, k_{IC} is the rate constant of internal conversion; k_{TADF}, k_{ISC}, k_{RISC} are the rate constant of TADF, intersystem crossing and reverse intersystem crossing, respectively. Φ_{ISC} and Φ_{RISC} are the quantum efficiencies of ISC and RISC process, respectively.

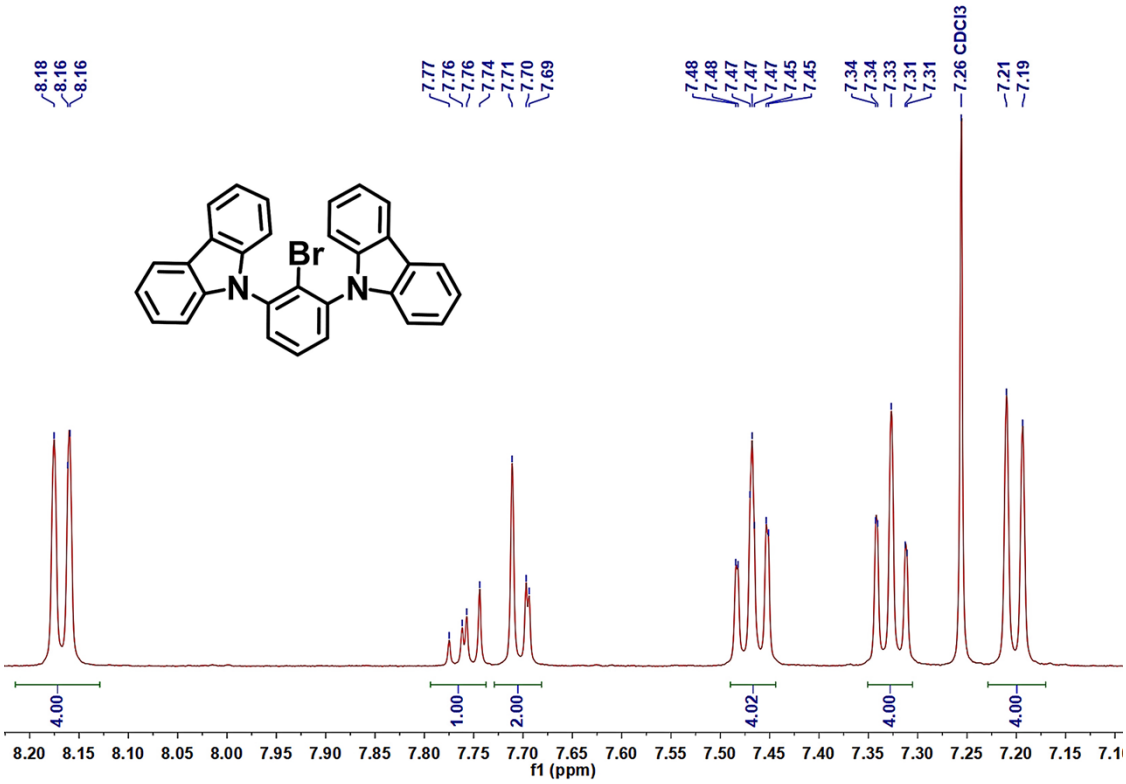

Figure S1. ^{1}H NMR spectrum (500 MHz, $CDCl_3$) of DCzBr.

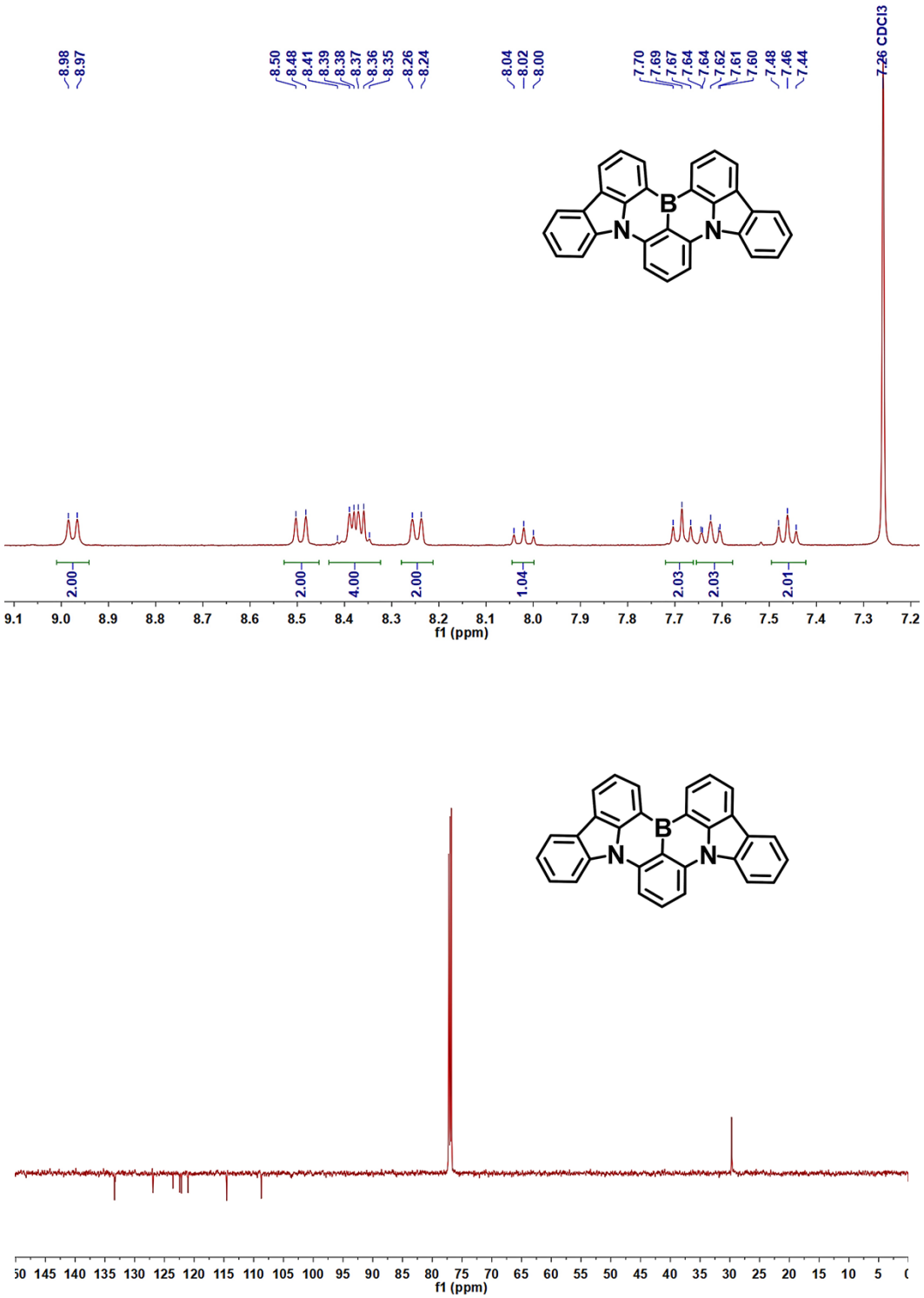

Figure S2. ^{1}H NMR spectrum (500 MHz, $CDCl_3$) and $^{13}C\{^{1}H\}$ NMR spectrum (151 MHz, $CDCl_3$) of DCzB.

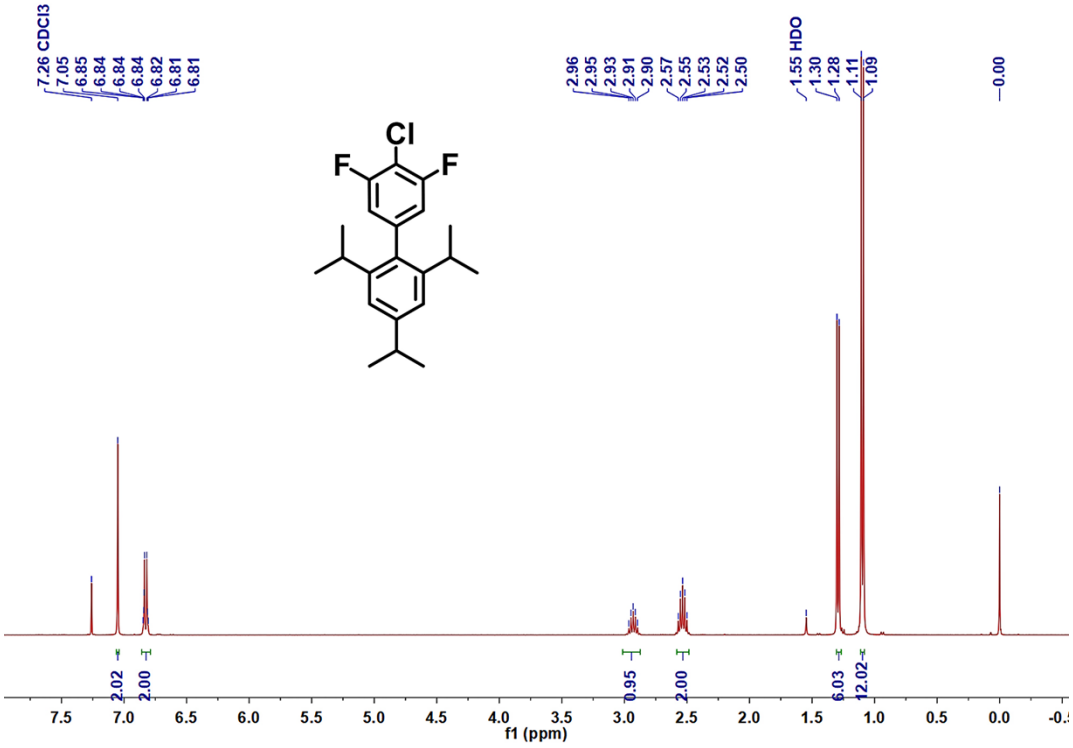

Figure S3. ^{1}H NMR spectrum (500 MHz, $CDCl_3$) of Tip-PhDFCl.

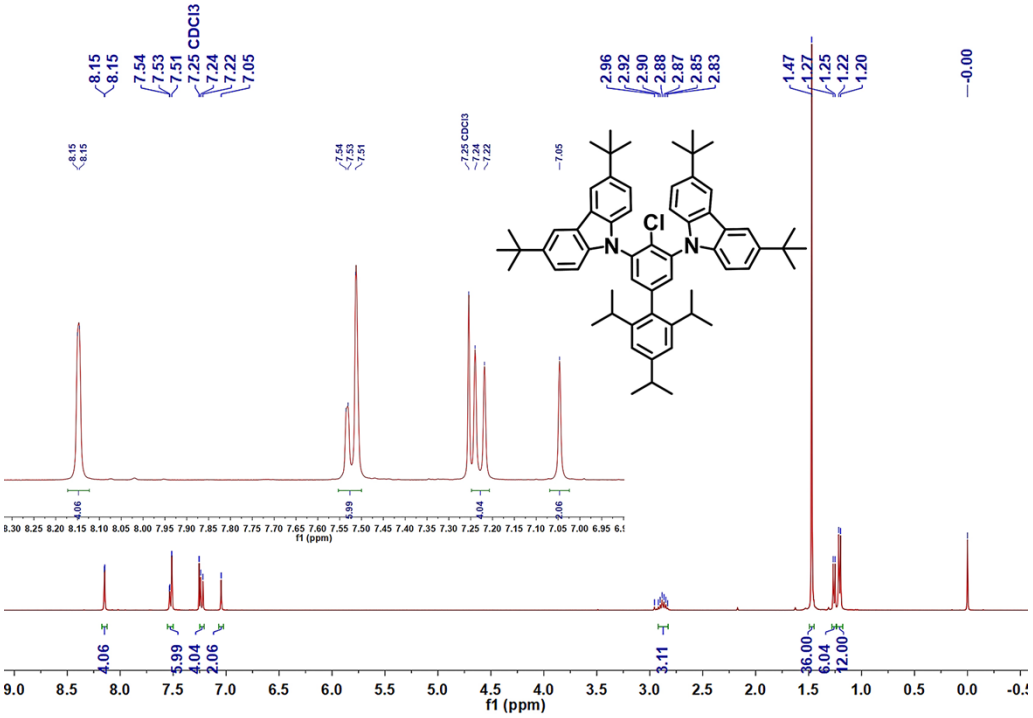

Figure S4. ^{1}H NMR spectrum (500 MHz, $CDCl_3$) of Tip-DtCzCl.

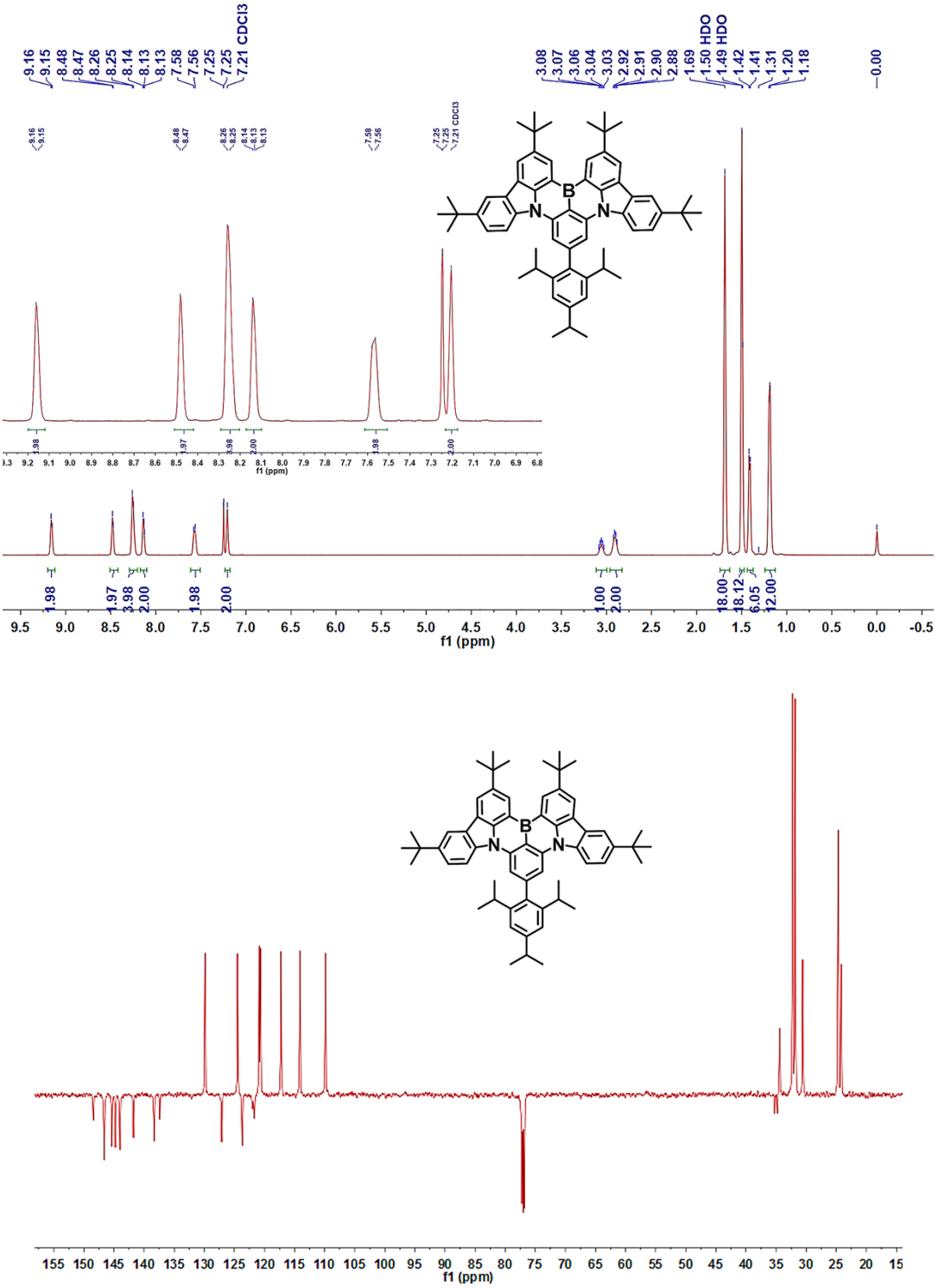

Figure S5. ^{1}H NMR spectrum (500 MHz, $CDCl_3$) and $^{13}C\{^{1}H\}$ NMR spectrum (151 MHz, $CDCl_3$) of Tip-DtCzB.

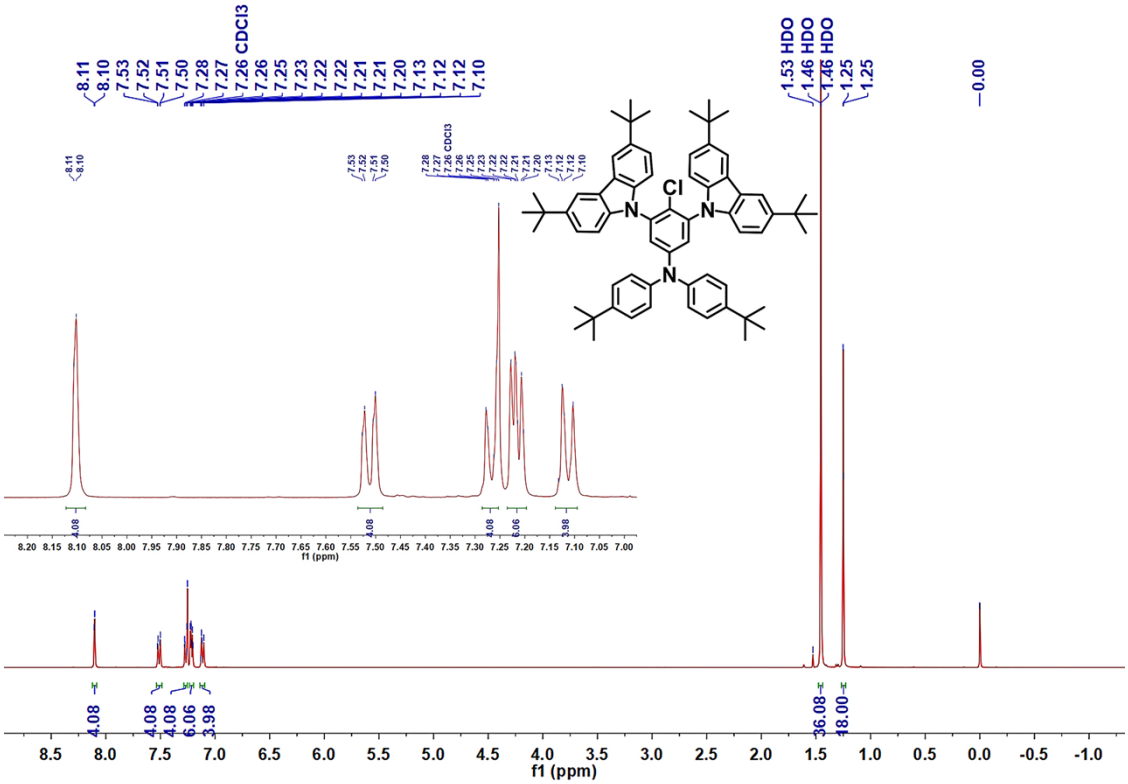

Figure S6. ^{1}H NMR spectrum (500 MHz, $CDCl_3$) of tDPA-DtCzCl.

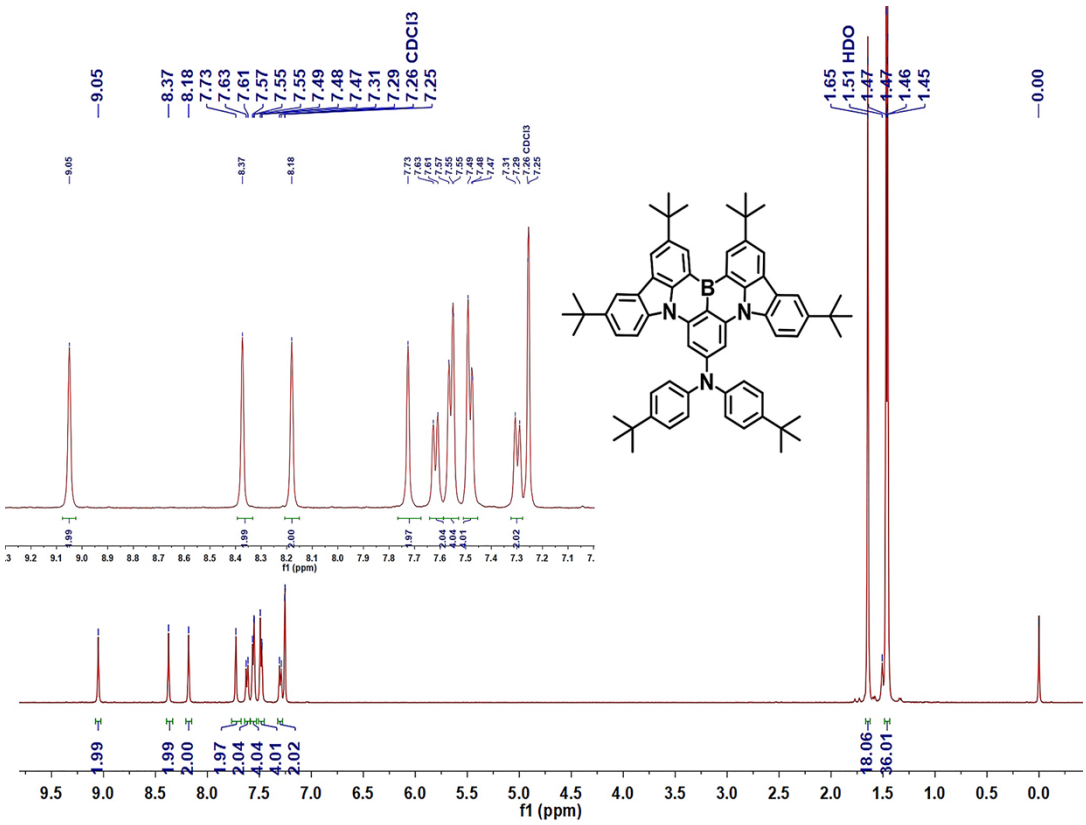

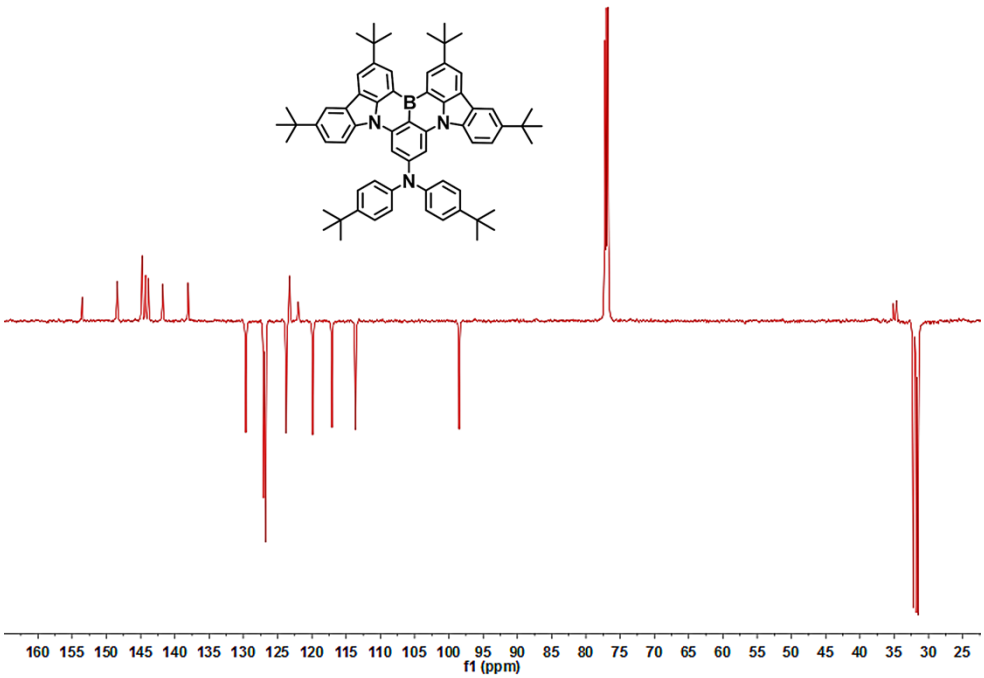

Figure S7. ^{1}H NMR spectrum (500 MHz, $CDCl_3$) and $^{13}C\{^{1}H\}$ NMR spectrum (151 MHz, $CDCl_3$) of tDPA-DtCzB.

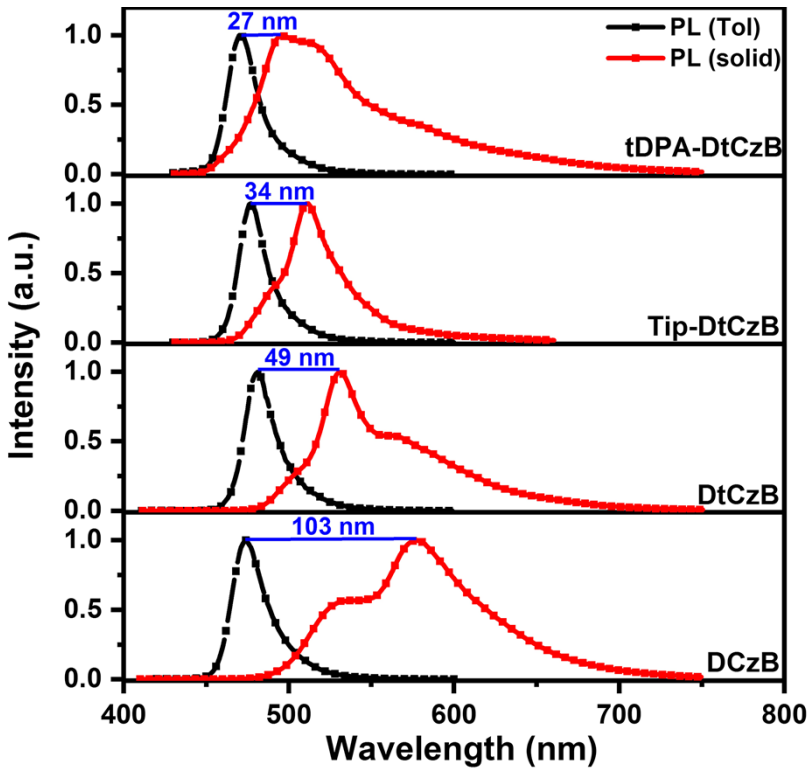

Figure S8. PL spectra of DCzB, DtCzB, Tip-DtCzB and tDPA-DtCzB in toluene solution (1×10^{-5} M, 298 K) and

solid state, respectively.

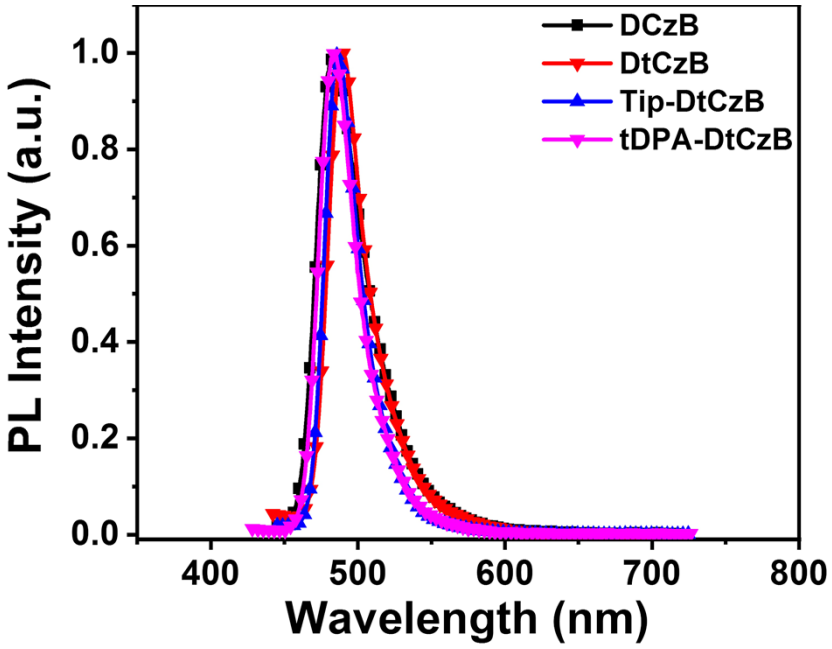

Figure S9. PL spectra of 1 wt% doping concentration of the investigated compounds in PhCzBCz deposited films.

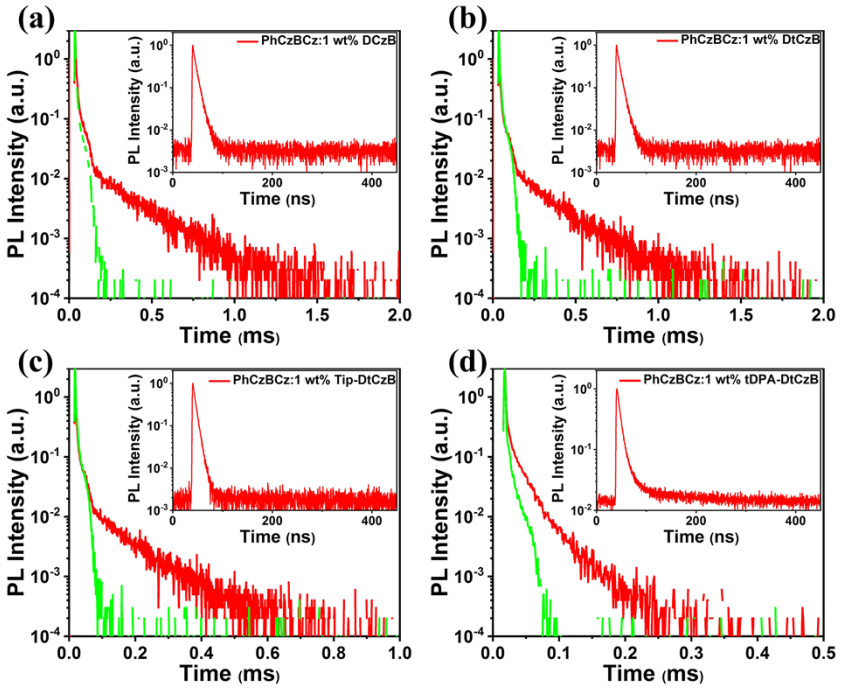

Figure S10. Transient PL decay curves recorded at 298 K and under vacuum atmosphere of 1 wt% doping concentration of DCzB (a), DtCzB (b), Tip-DtCzB (c) and tDPA-DtCzB (d) in PhCzBCz deposited films.

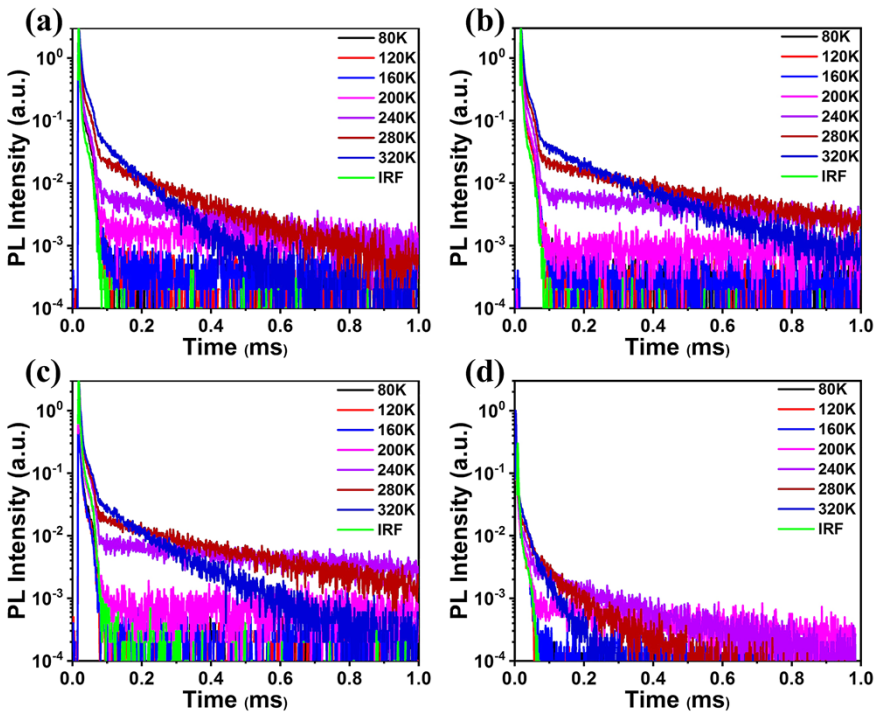

Figure S11. Variable-temperature transient PL decay curves of 1 wt% doping concentration of DCzB (a), DtCzB (b), Tip-DtCzB (c) and tDPA-DtCzB (d) in PhCzBCz deposited films.

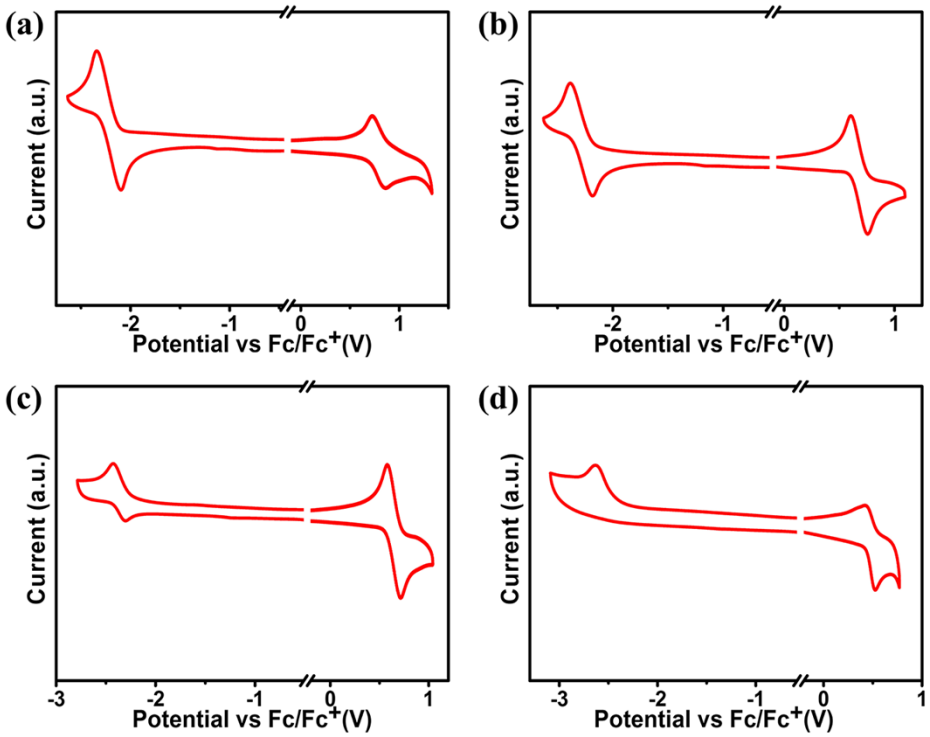

Figure S12. CV curves of DCzB (a), DtCzB (b), Tip-DtCzB (c) and tDPA-DtCzB (d).

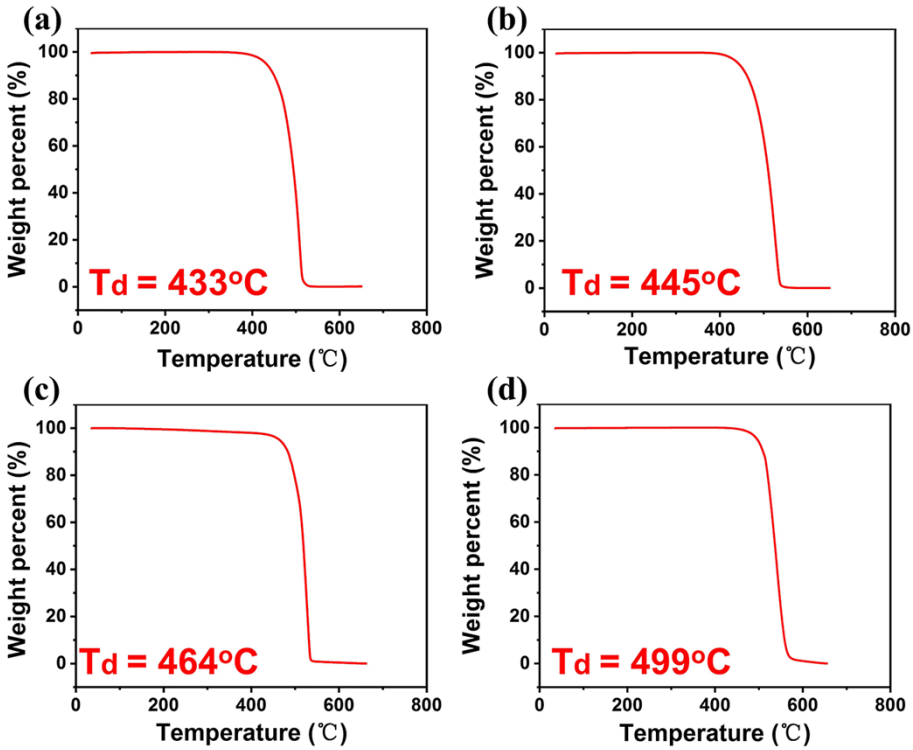

Figure S13. TGA curves of DCzB (a), DtCzB (b), Tip-DtCzB (c) and tDPA-DtCzB (d).

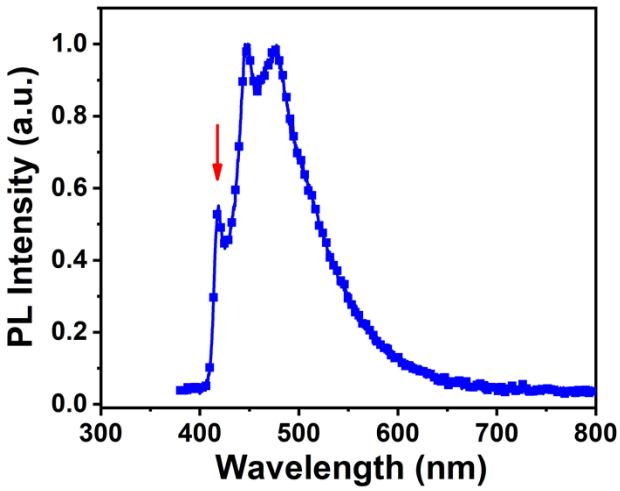

Figure S14. Phosphorescence spectra (77 K) of PhCzBCz measured in toluene (1×10^{-5} M).

E_{T1} = 1240 / 418.6 = 2.96 eV.

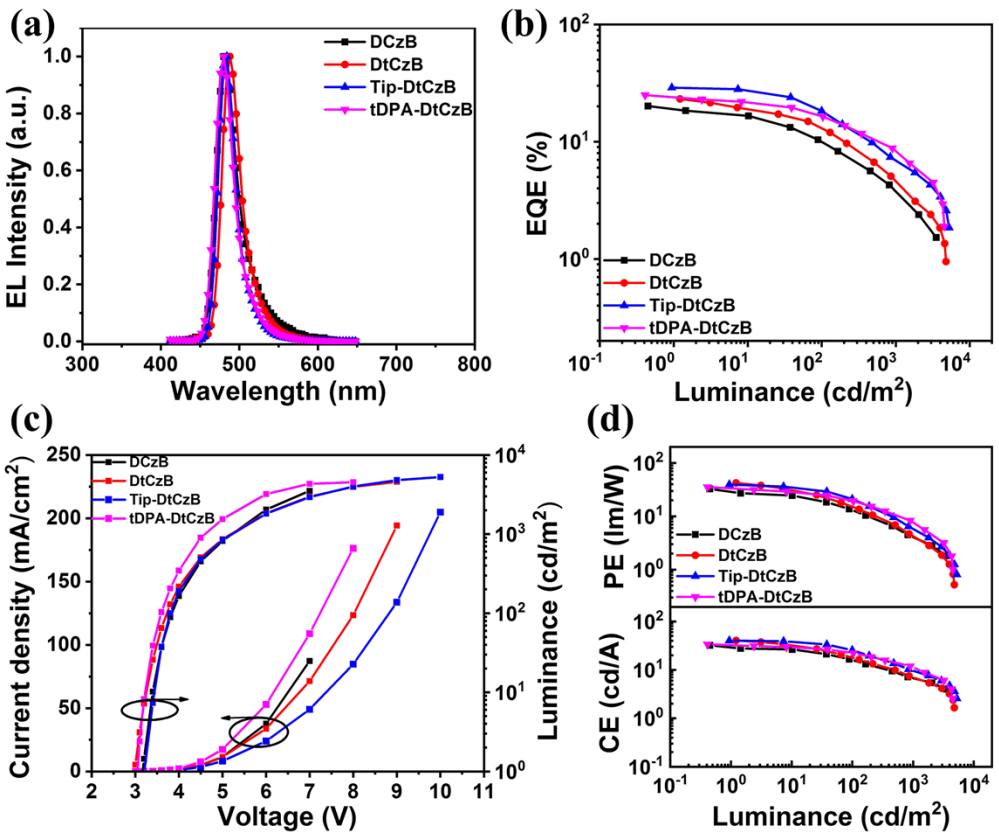

Figure S15. EL characteristics of the devices with the configuration of ITO/TAPC (50 nm)/TCTA (5 nm)/PhCzBCz: 1 wt% the investigated compounds (30 nm)/TmPyPB (30 nm)/LiF (1 nm)/Al (100 nm). a) EL spectra. b) EQE-*L* curves. c) *J*-*V*-*L* curves. d) CE-*L* and PE-*L* curves.

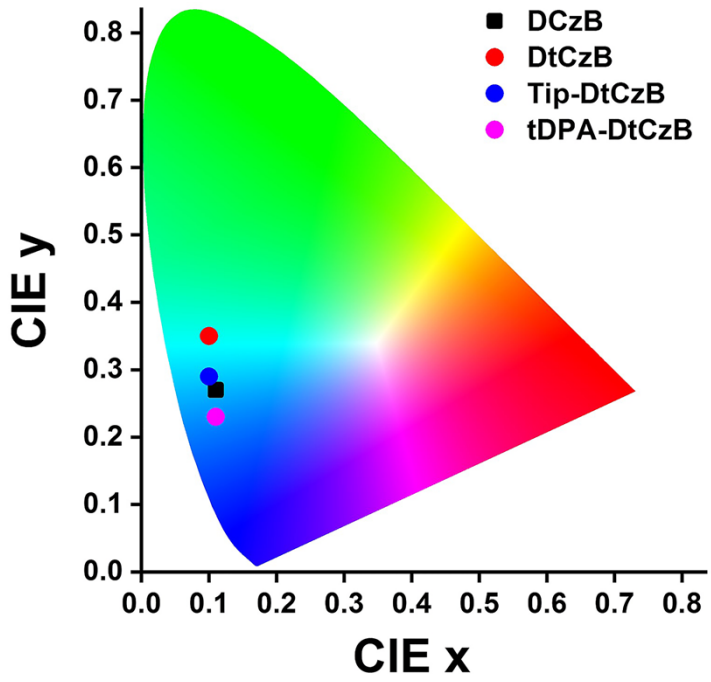

Figure S16. Color coordinates of the investigated compounds-based devices (1 wt% doping concentration) on the CIE 1931 color space.

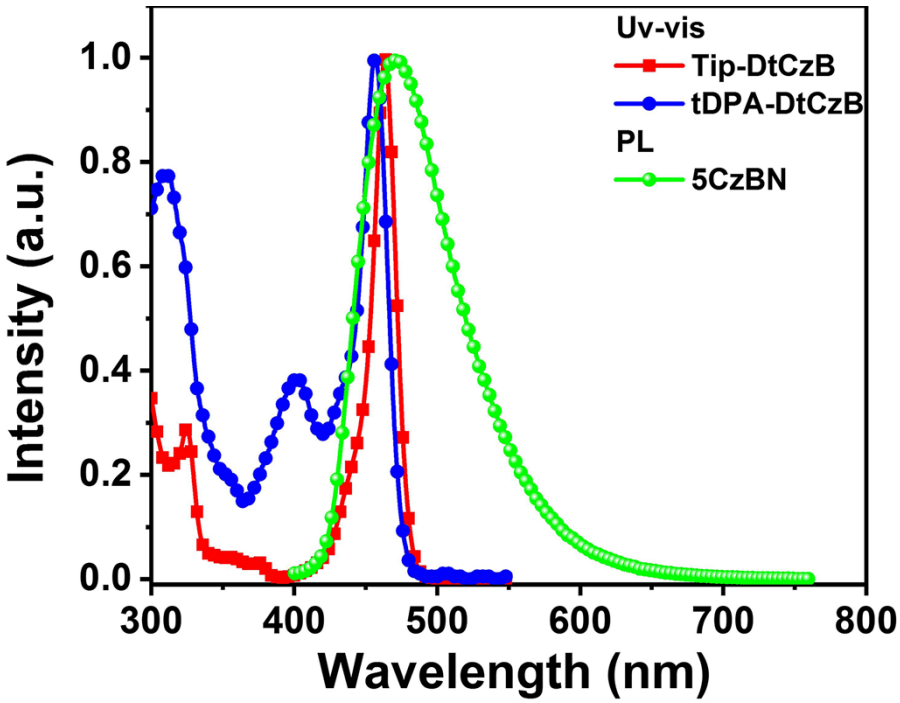

Figure S17. UV–vis absorption spectra of Tip-DtCzB, tDPA-DtCzB and PL spectrum of 5CzBN in toluene solution (1×10^{-5} M, 298 K).

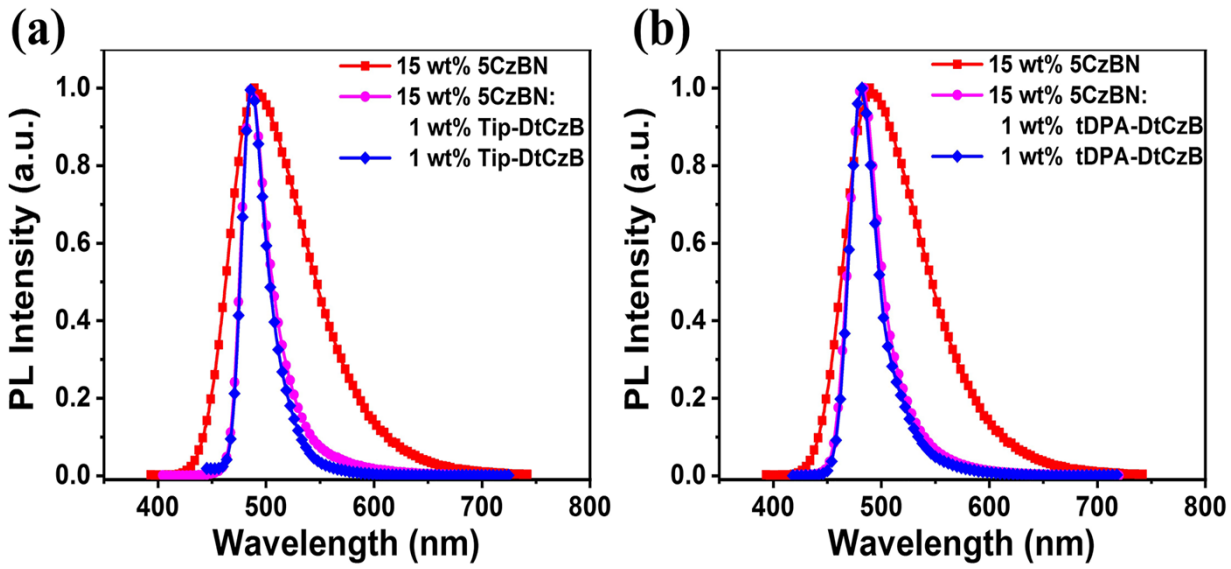

Figure S18. PL spectra of 15 wt% 5CzBN, 15 wt% 5CzBN: 1 wt% Tip-DtCzB, 1 wt% Tip-DtCzB (a) and 15 wt% 5CzBN, 15 wt% 5CzBN:1 wt% tDPA-DtCzB, 1 wt% tDPA-DtCzB (b) in PhCzBCz deposited films.

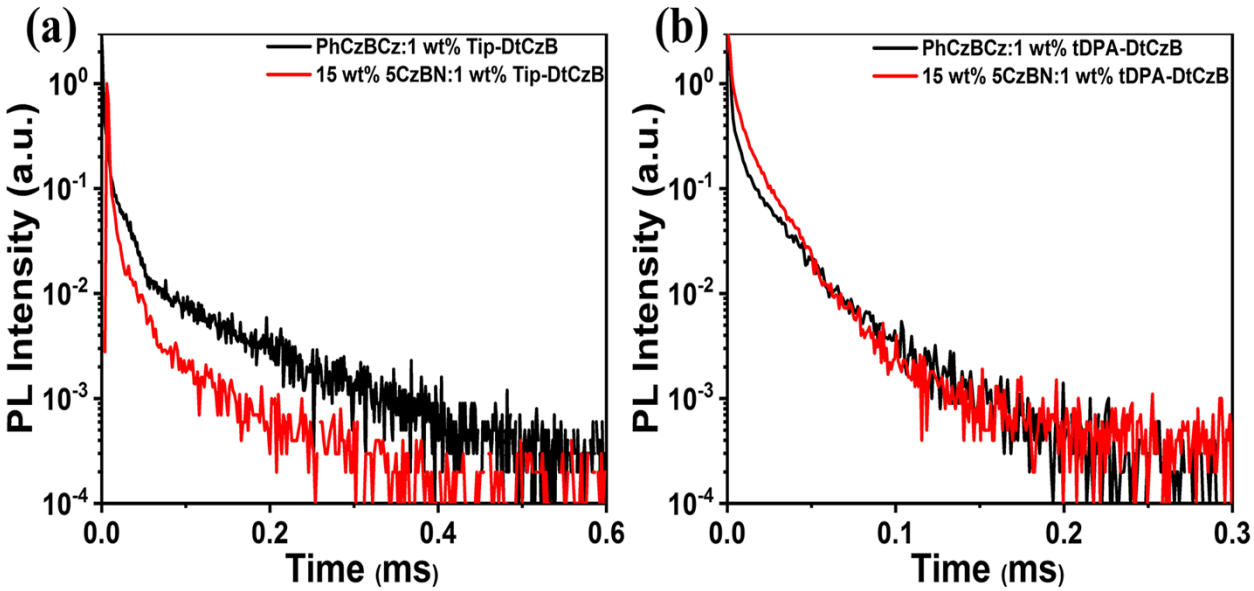

Figure S19. Transient PL decay curves of PhCzBCz: 1 wt% Tip-DtCzB, PhCzBCz: 15 wt% 5CzBN: 1 wt% Tip-DtCzB (a) and PhCzBCz: 1 wt% tDPA-DtCzB, PhCzBCz: 15 wt% 5CzBN: 1 wt% tDPA-DtCzB (b) films.

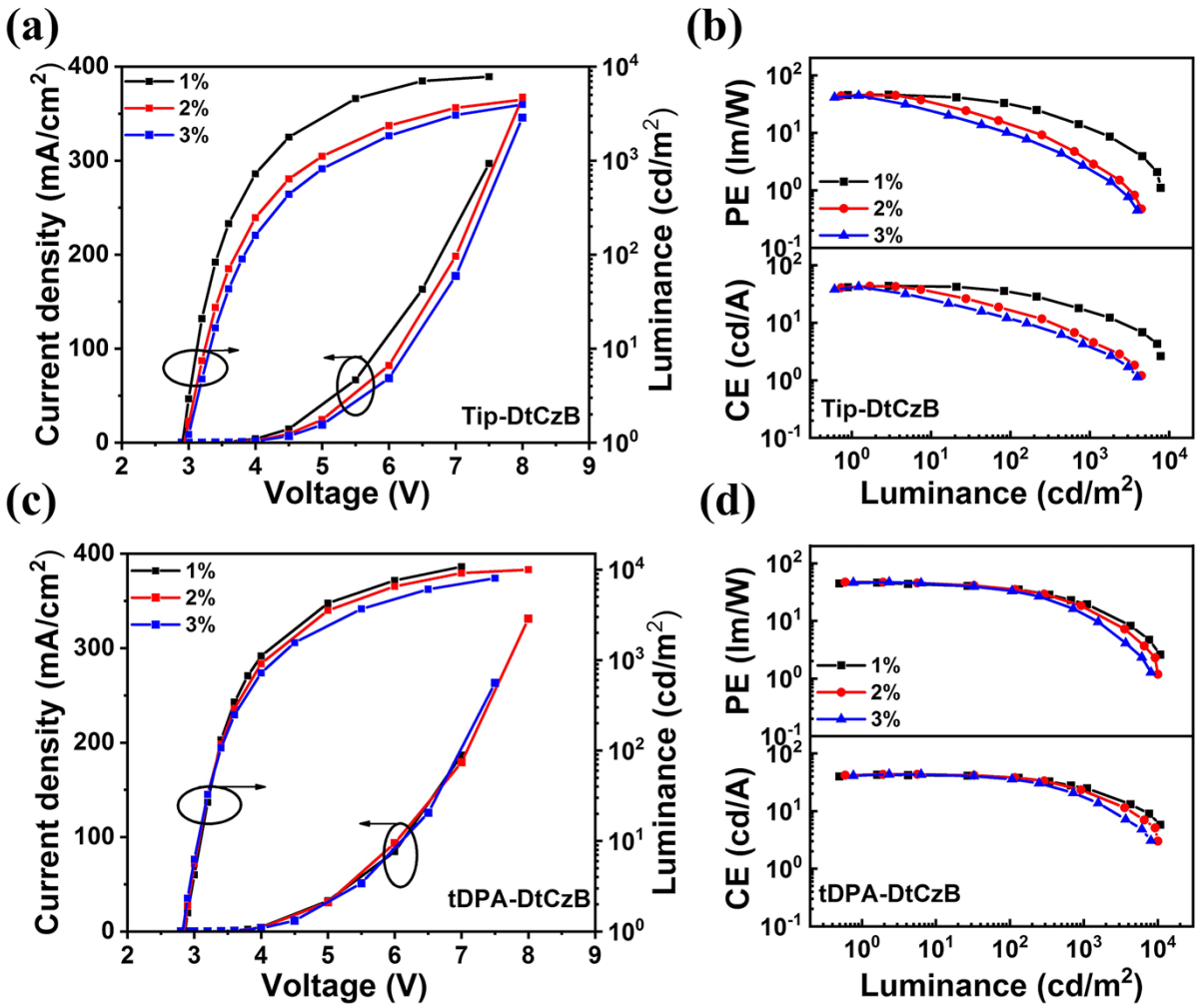

Figure S20. EL characteristics of the devices with the configuration of ITO/TAPC (50 nm)/TCTA (5 nm)/PhCzBCz: 15 wt% 5CzBN: x wt% Tip-DtCzB or tDPA-DtCzB (30 nm)/TmPyPB (30 nm)/LiF (1 nm)/Al (100 nm) (x = 1, 2, 3). a, c) *J*-*V*-*L* curves. b, d) CE-*L* and PE-*L* curves.

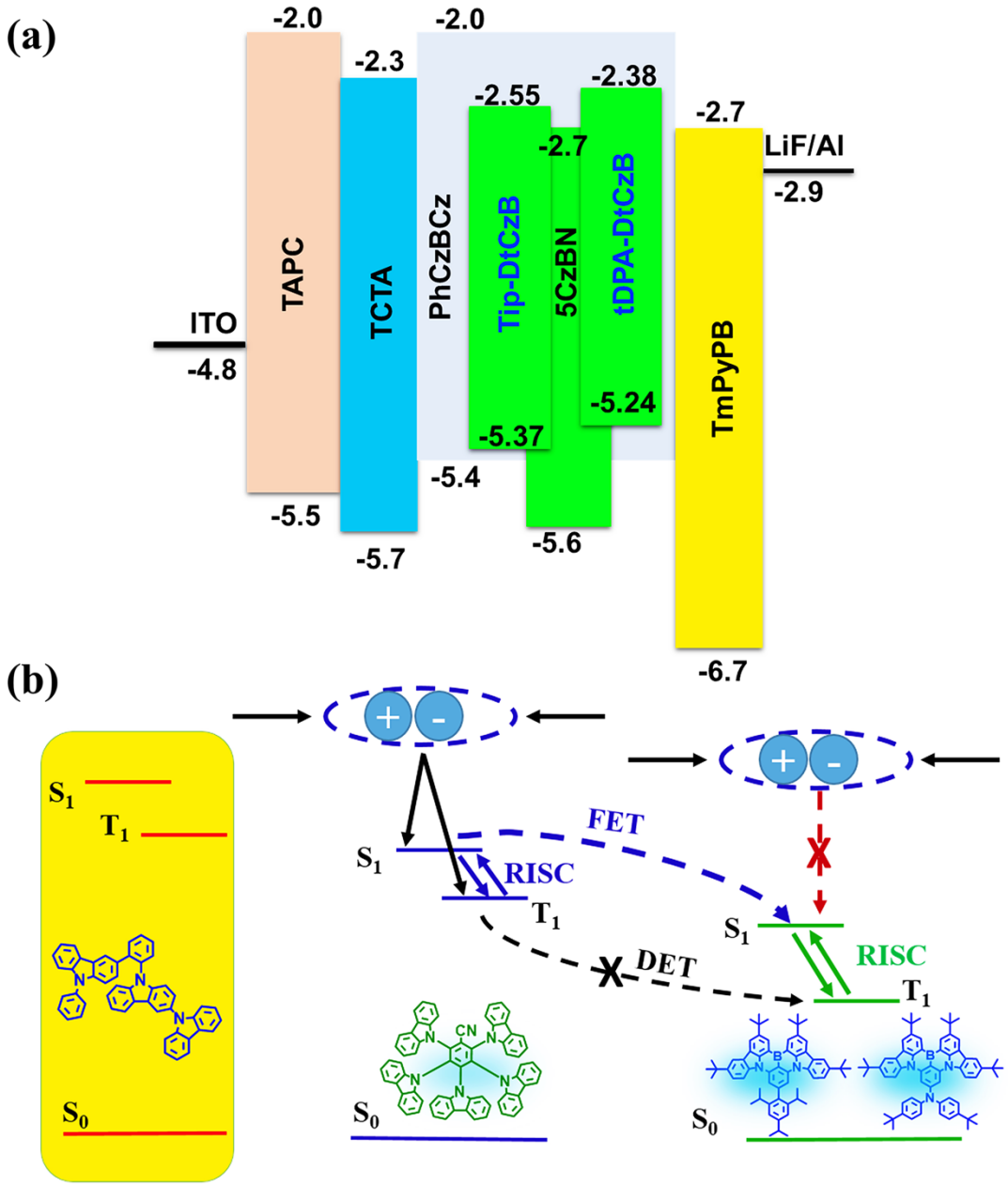

Figure S21. Schematic illustration of energy transfer mechanism in the EML consisting of PhCzBCz: 5CzBN: fluorescent dye under electrical excitation.

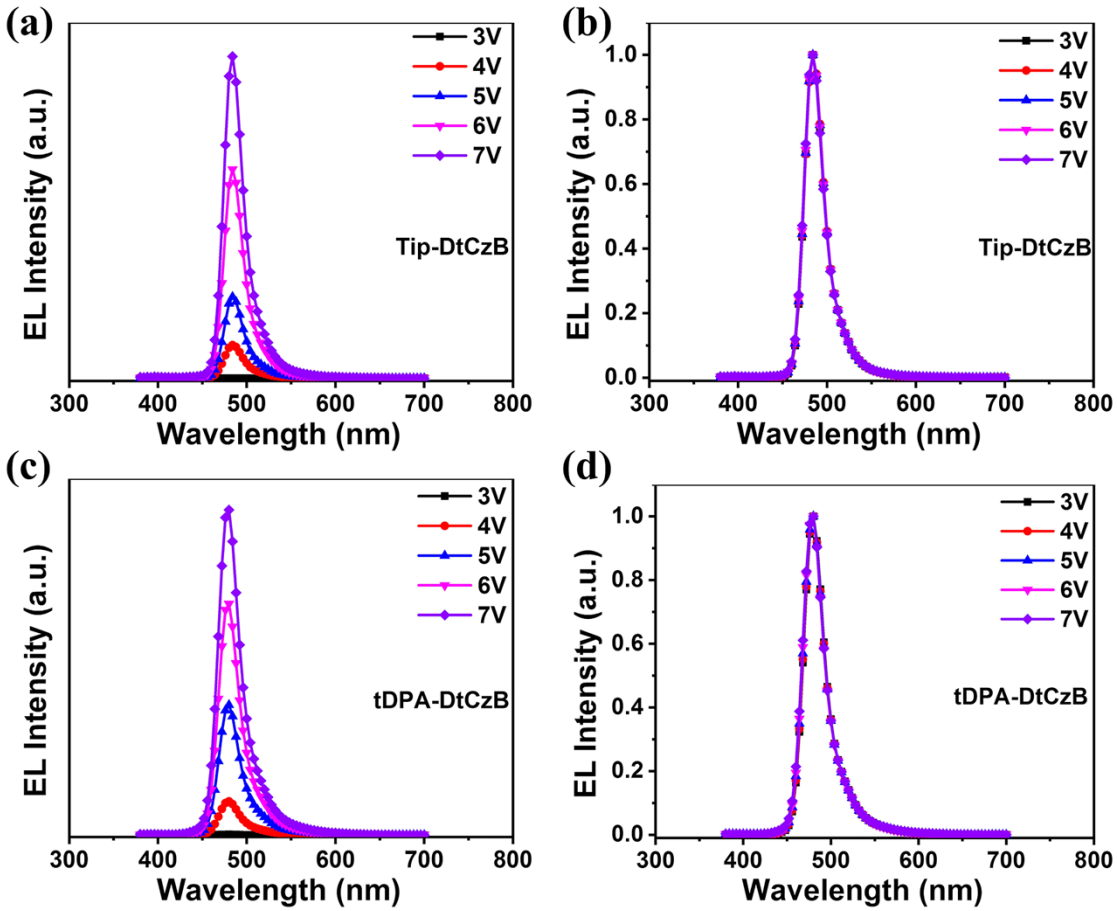

Figure S22. Original (a, c) and normalized (b, d) EL spectra operated at different voltages of Tip-DtCzB- and tDPA-DtCzB-based devices (1 wt% doping concentration) with 5CzBN sensitizer.

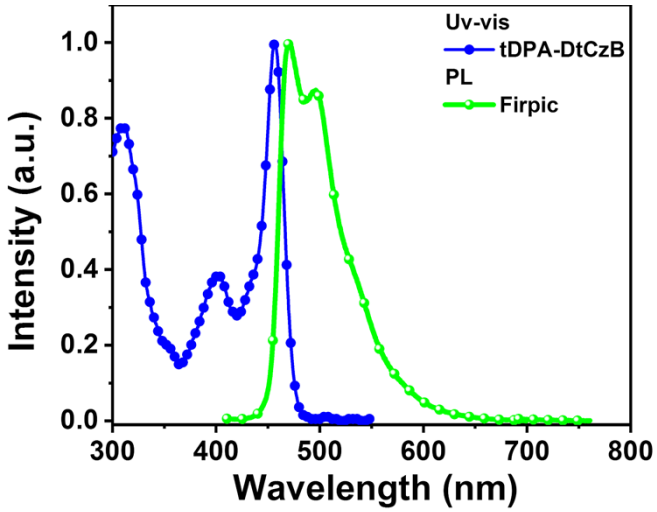

Figure S23. UV–vis absorption spectrum of tDPA-DtCzB and PL spectrum of Firpic in toluene solution (1×10^{-5} M, 298 K).

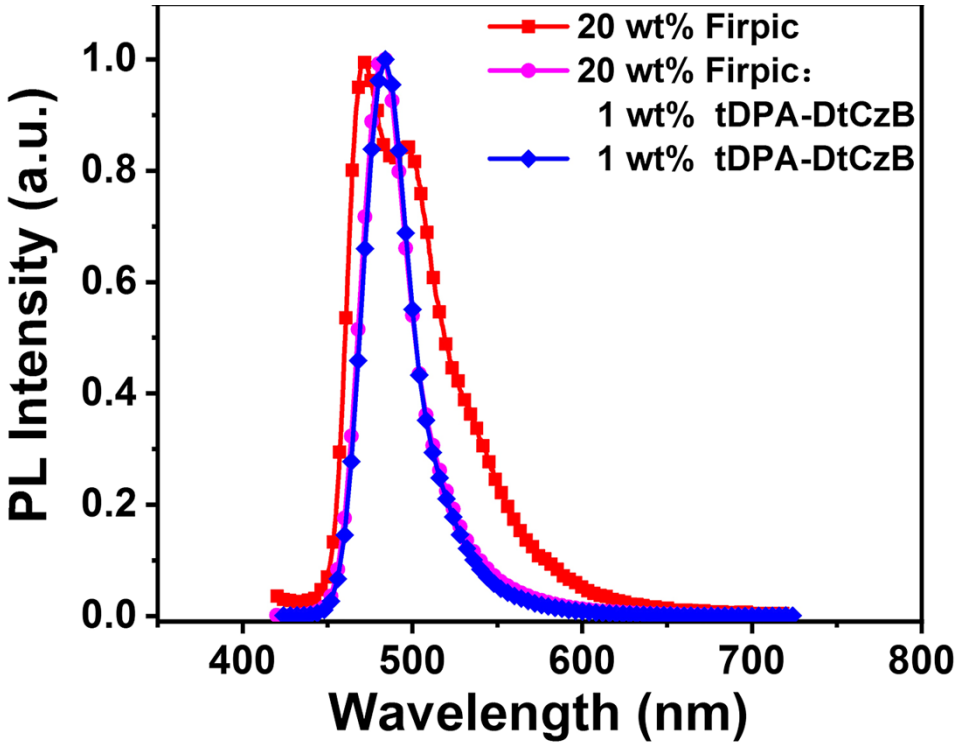

Figure S24. PL spectra of 20 wt% Firpic, 20 wt% Firpic: 1 wt% tDPA-DtCzB, 1 wt% tDPA-DtCzB in PhCzBCz deposited films.

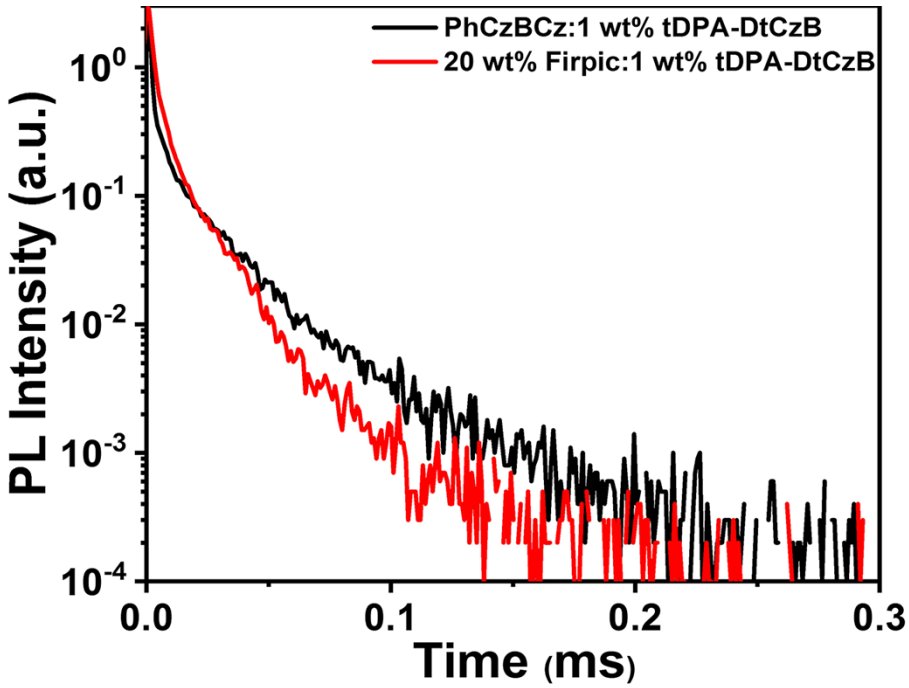

Figure S25. Transient PL decay curves of PhCzBCz: 1 wt% tDPA-DtCzB and PhCzBCz: 20 wt% Firpic: 1 wt% tDPA-DtCzB films.

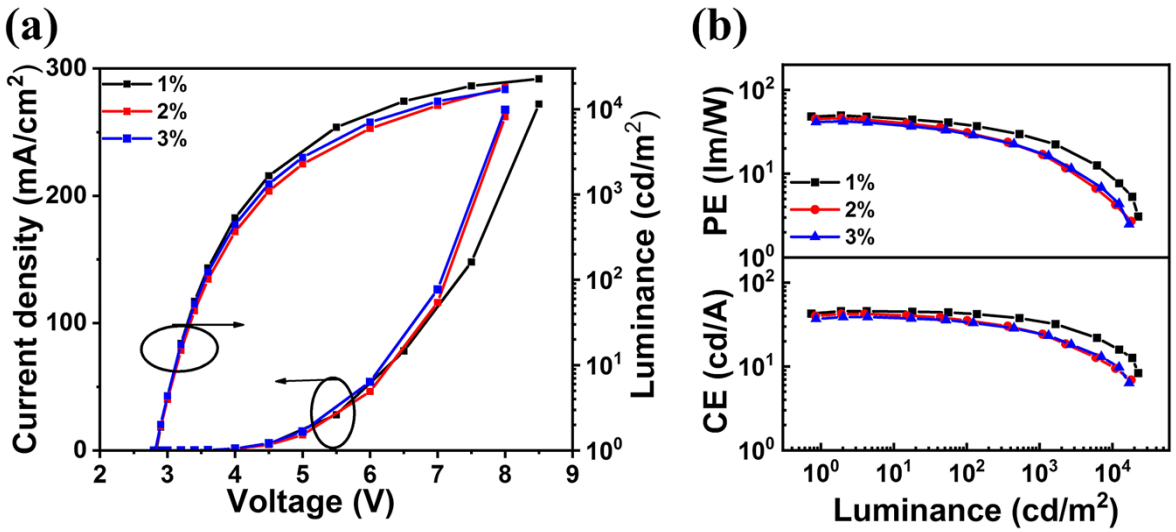

Figure S26. EL characteristics of the devices with the configuration of ITO/TAPC (50 nm)/TCTA (5 nm)/PhCzBCz: 20 wt% Firpic: x wt% the investigated compounds (30 nm)/TmPyPB (30 nm)/LiF (1 nm)/Al (100 nm) (x = 1, 2, 3). a) *J*-*V*-*L* curves. b) CE-*L* and PE-*L* curves.

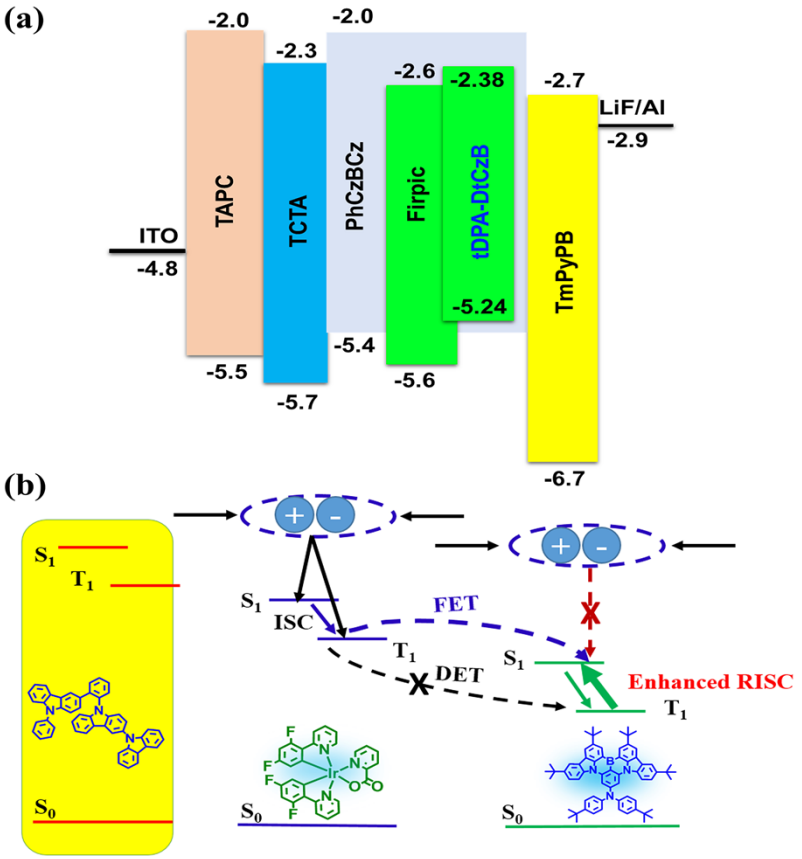

Figure S27. Schematic illustration of energy transfer mechanism in the EML consisting of PhCzBCz: Firpic: fluorescent dye under electrical excitation.

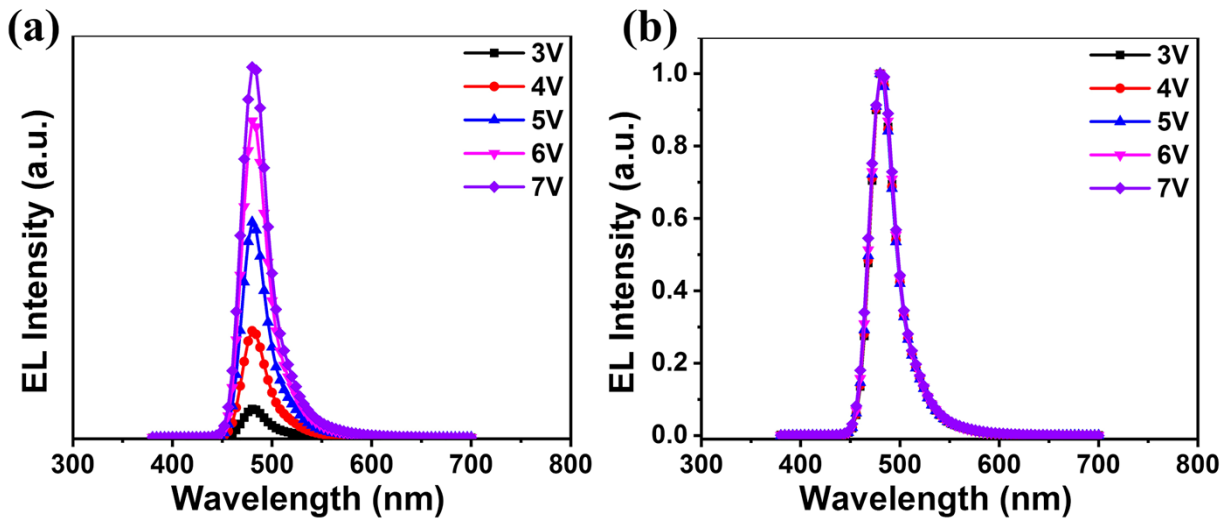

Figure S28. Original (a) and normalized (b) EL spectra operated at different voltages of tDPA-DtCzB-based device (1 wt% doping concentration) with Firpic sensitizer.

Table S1. Summary of PL spectra data of 1 wt% doping concentration of the investigated compounds in PhCzBCz deposited films.

compound	λ_{em}[a)] [nm]	FWHM[b)] [nm]
DCzB	484	36
DtCzB	490	31
Tip-DtCzB	486	29
tDPA-DtCzB	484	30

[a)] PL peak wavelength. [b)] Full width at half maximum.

Table S2. Summary of photophysical data of 1 wt% doping concentration of the investigated compounds in PhCzBCz deposited films.

dopant	DCzB	DtCzB	Tip-DtCzB	tDPA-DtCzB	5CzBN: Tip-DtCzB	5CzBN: tDPA-DtCzB	Firpic: tDPA-DtCzB
Φ_{PL}[a] [%]	78	89	95	85	96	88	92
Φ_{F}[b] [%]	67.9	76.5	80.8	63.8	68.2	51.9	46.9
Φ_{TADF}[c] [%]	10.1	12.5	14.3	21.2	27.8	36.1	45.1
τ_{F}[d] [ns]	8.4	6.8	5.6	7.7	7.6	9.2	2.5
Ref_{F}[e] [%]	87	86	85	75	71	59	51
τ_{TADF}[f] [μs]	122.8	106.6	100.0	29.5	28.3	19.4	14.8
Ref_{TADF}[g] [%]	13	14	15	25	29	41	49
k_{F}[h] [10^7 s^{-1}]	8.08	11.25	14.43	8.29	8.97	5.64	18.76
k_{IC}[i] [10^7 s^{-1}]	2.28	1.39	0.76	1.46	0.37	0.77	1.63
k_{ISC}[j] [10^7 s^{-1}]	1.54	2.07	2.67	3.24	3.81	4.46	19.61
k_{TADF}[k] [10^4 s^{-1}]	0.64	0.83	0.96	2.88	3.39	4.54	6.22
k_{RISC}[l] [10^4 s^{-1}]	0.50	0.74	0.92	2.45	3.26	3.99	5.72
Φ_{ISC}[m] [%]	12.95	14.04	14.95	24.94	28.96	41.02	49.02

[a] The total photoluminescence quantum yield (Φ_{PL}). [b] The prompt fluorescent (Φ_{F}) component of Φ_{PL}. [c] The delayed fluorescent (Φ_{TADF}) component of Φ_{PL}. [d] The lifetime of prompt fluorescence (τ_{F}). [e] The proportion of prompt fluorescence lifetime. [f] The lifetime of delayed fluorescence (τ_{TADF}). [g] The proportion of delayed fluorescence lifetime. [h] The rate constant of prompt fluorescence (k_{F}). [i] The rate constant of internal conversion (k_{IC}). [j] The rate constant of TADF (k_{TADF}). [k] The rate constant of intersystem crossing (k_{ISC}). [l] The rate constant of reverse intersystem crossing (k_{RISC}). [m] The efficiency of ISC(Φ_{ISC}).

Table S3. Summary of the EL data of the investigated compounds-based devices.

compound	λ_{em}[a] [nm]	FWHM[b] [nm]	V_{on}[c] [V]	L_{max}[d] [cd m^{-2}]	CE_{max}[e] [cd A^{-1}]	PE_{ma}[f] [lm W^{-1}]	EQE[g] [%]	CIE(x, y)[h]
DCzB	480	30	3.2	3523	32.2	32.7	20.2/9.9/3.7	(0.11, 0.27)
DtCzB	488	27	3.1	4783	40.4	42.3	23.2/13.0/4.6	(0.10, 0.35)
Tip-DtCzB	484	25	3.2	5266	40.3	40.8	28.9/18.2/6.8	(0.10, 0.29)
tDPA-DtCzB	480	27	3.1	4533	31.0	31.5	25.0/16.4/8.3	(0.11, 0.23)

[a] EL peak wavelength. [b] Full width at half maximum. [c] Turn-on voltage at 1 cd m^{-2}. [d] Maximum luminance. [e] Maximum current efficiency. [f] Maximum power efficiency. [g] Maximum external quantum efficiency, and values at 100 and 1000 cd m^{-2}, respectively. [h] Value taken at 100 cd m^{-2}.

References

(1) A. D. Becke, *J. Chem. Phys.* **1993**, *98*, 5648–5652.

(2) C. Lee, W. Yang, R. G. Parr, *Phys. Rev. B* **1988**, *37*, 785–789.

(3) R. Krishnan, J. S. Binkley, R. Seeger, J. Pople, *J. Chem. Phys.* **1980**, 72, 650–654.

(4) S. Grimme, J. Antony, S. Ehrlich, H. Krieg, *J. Chem. Phys.* **2010**, *132*, 154104.

(5) Gaussian 09, Revision D.01, M. J. Frisch, G. W. Trucks, H. B. Schlegel, G. E. Scuseria, M. A. Robb, J. R. Cheeseman, G. Scalmani, V. Barone, B. Mennucci, G. A. Petersson, H. Nakatsuji, M. Caricato, X. Li, H. P. Hratchian, A. F. Izmaylov, J. Bloino, G. Zheng, J. L. Sonnenberg, M. Hada, M. Ehara, K. Toyota, R. Fukuda, J. Hasegawa, M. Ishida, T. Nakajima, Y. Honda, O. Kitao, H. Nakai, T. Vreven, J. A. Montgomery, Jr., J. E. Peralta, F. Ogliaro, M. Bearpark, J. J. Heyd, E. Brothers, K. N. Kudin, V. N. Staroverov, T. Keith, R. Kobayashi, J. Normand, K. Raghavachari, A. Rendell, J. C. Burant, S. S. Iyengar, J. Tomasi, M. Cossi, N. Rega, J. M. Millam, M. Klene, J. E. Knox, J. B. Cross, V. Bakken, C. Adamo, J. Jaramillo, R. Gomperts, R. E. Stratmann, O. Yazyev, A. J. Austin, R. Cammi, C. Pomelli, J. W. Ochterski, R. L. Martin, K. Morokuma, V. G. Zakrzewski, G. A. Voth, P. Salvador, J. J. Dannenberg, S. Dapprich, A. D. Daniels, O. Farkas, J. B. Foresman, J. V. Ortiz, J. Cioslowski, and D. J. Fox, Gaussian, Inc., Wallingford CT, **2013**.

(6) Y. Xu, Z. Cheng, Z. Li, B. Liang, J. Wang, J. Wei, Z. Zhang, Y. Wang, *Adv. Opt. Mater.* **2020**, *8*, 1902142.

(7) Y. Zhang, D. Zhang, J. Wei, Z. Liu, Y. Lu, L. Duan, *Angew. Chem. Int. Ed.* **2019**, *58*, 16912–16917; *Angew. Chem.* **2019**, *131*, 17068–17073.

(8) Q. Zhang, H. Kuwabara, W. J. Potscavage, S. Huang, Y. Hatae, T. Shibata, C. Adachi, *J. Am. Chem. Soc.* **2014**, *136*, 18070–18081.

(9) Q. Zhang, B. Li, S. Huang, H. Nomura, H. Tanaka, C. Adachi, *Nat. Photonics* **2014**, *8*, 326–332.

(10) T.-L. Wu, M.-J. Huang, C.-C. Lin, P.-Y. Huang, T.-Y. Chou, R.-W. Chen-Cheng, H.-W. Lin, R.-S. Liu, C.-H. Cheng, *Nat. Photonics* **2018**, *12*, 235–240.

(11) T. Hatakeyama, K. Shiren, K. Nakajima, S. Nomura, S. Nakatsuka, K. Kinoshita, J. Ni, Y. Ono, T. Ikuta, *Adv. Mater.* **2016**, *28*, 2777–2781.